科学通报 2018 年 第 63 卷 第 8 期: 766 ~ 776
论 文
《中国科学》杂志社
SCIENCE CHINA PRESS

忽略 1.6 μm 偏振计算对二氧化碳反演精度的影响

白文广[1,2], 张鹏[2*], 张文建[2], 马刚[2], 漆成莉[2], 刘辉[2]

1. 南京信息工程大学大气物理学院, 南京 210044;
2. 国家卫星气象中心, 北京 100081
* 联系人, E-mail: zhangp@cma.gov.cn

2017-08-04 收稿, 2018-01-02 修回, 2018-01-04 接受, 2018-03-12 网络版发表
国家高技术研究发展计划(2015AA123704, 2011AA12A104)、国家自然科学基金(41475031)和公益性行业(气象)科研专项(GYHY201506074, GYHY201506002)资助

摘要 散射引起的偏振效应会对卫星遥感二氧化碳精度产生较大的影响. 本文利用逐线积分方法和累加法精确模拟了星载仪器近红外1.6 μm波段的大气层顶偏振辐射特征, 计算了分子散射和气溶胶散射引入的偏振效应, 分析了偏振效应对大气二氧化碳反演精度的影响. 研究表明: 1.6 μm波段散射引入的偏振效应明显, 并随太阳高度角、观测天顶角、气溶胶光学厚度、地表反射率而变化. 除个别大角度观测天顶角外, 偏振效应随太阳天顶角升高、气溶胶光学厚度增加、地表反射率的减小而变大, 并且在吸收线位置的影响要高于窗区. 忽略偏振效应导致的大气二氧化碳反演误差随太阳天顶角的升高、气溶胶光学厚度的增加以及地表反照率减小而增大, 并且该误差与仪器观测角度有关. 模拟结果显示在高太阳天顶角、高气溶胶光学厚度以及低反照率场景下, 忽略偏振计算可能引入高于10 ppmv(1 ppmv=10^{-6} L/L)反演误差, 远高于1~2 ppmv观测需求. 为减小误差, 基于该波段的二氧化碳反演需要考虑大气辐射偏振的影响.

关键词 矢量辐射传输计算, 卫星近红外 1.6 μm 观测, 二氧化碳反演误差

二氧化碳(CO_2)是大气中人为活动影响的主要温室气体成分, 其在大气中的浓度变化是影响全球气候变化、全球碳循环等研究的主要不确定因素. 进入21世纪, 随着星载高光谱遥感技术的成熟, 卫星遥感全球大气中CO_2的含量已经成为一种非常重要的观测手段, 如日本2009年发射的GOSAT卫星、美国2014年发射的OCO-2卫星、我国2016年发射的碳卫星等. 这3颗卫星均可通过O_2 A带(0.76 μm)、近红外CO_2弱吸收带(1.6 μm)以及CO_2强吸收带(2.06 μm)联合观测探测地表气压、云高以及大气中温室气体CO_2信息[1,2].

入射地球的自然太阳光本身没有偏振特征, 由于大气散射(大气分子、气溶胶和云滴粒子)和地表反射的偏振特征作用, 使得卫星观测的大气层顶出射光谱辐射具有了偏振特征. 有研究表明, 短波波段偏振辐射效应明显, 不仅不能忽视, 还可以提供遥感大气的额外信息, 国际上已经用于对流层臭氧、卷云、气溶胶的探测[3~8]. 美国OCO-2以及我国碳卫星搭载的光谱仪采用光栅分光, 通过跟踪主平面方式探测与主平面垂直的电矢量分量信号, 是典型的偏振敏感性仪器. 其中短波红外1.6和2.06 μm波段用于探测CO_2柱浓度; 0.76 μm波段主要用于探测O_2柱浓度, 对CO_2柱浓度进行路径修正得到干空气混合比XCO_2(XCO_2=0.2095×(CO_2柱总量/O_2柱总量))[9,10]. 相比2.06 μm波段, 0.76 μm波段对分子散射、1.6 μm波段对气溶胶散射更为敏感, 偏振效应比较明显, 在观测资料处理中需要考虑偏振效应的影响.

引用格式: 白文广, 张鹏, 张文建, 等. 忽略 1.6 μm 偏振计算对二氧化碳反演精度的影响. 科学通报, 2018, 63: 766–776
Bai W G, Zhang P, Zhang W J, et al. CO_2 column-retrieval errors arising from neglecting polarization in forward modeling of 1.6 μm band measurements (in Chinese). Chin Sci Bull, 2018, 63: 766–776, doi: 10.1360/N972017-00853

© 2018《中国科学》杂志社

偏振辐射传输计算是偏振观测数据处理的基础, Stam等人[11]通过辐射传输模拟计算, 理论分析了O_2 A带不同吸收光学厚度波长处的光谱偏振特性. 在此基础上, Natraj等人[12]以美国碳卫星为例对忽略O_2 A带偏振辐射传输计算可能导致的CO_2反演误差进行了分析评估, 指出忽略O_2 A带偏振计算可能引入高达10 ppmv(1 ppmv=10^{-6} L/L, 余同)的XCO_2反演误差, 远高于1~2 ppmv观测精度需求. 而近红外1.6 μm波段, 尽管相比0.76 μm波段, 分子散射作用变弱, 但气溶胶散射明显, 忽略偏振计算同样会造成观测辐射强度模拟误差, 并引入XCO_2反演误差. 目前这方面研究国内外开展的尚不充分. 本文针对1.6 μm波段偏振计算可能引起的XCO_2反演误差, 介绍了偏振辐射传输计算原理, 模拟分析忽略偏振计算导致的观测辐射强度计算误差, 通过敏感性模拟计算, 估算分析忽略1.6 μm波段偏振辐射传输计算可能导致的XCO_2反演误差.

1 偏振辐射传输计算

1.1 考虑偏振的辐射传输方程

忽略地气热辐射作用, 考虑偏振的单色平面平行大气辐射传输方程表示为[13~15]

$$\mu\frac{\mathrm{d}\boldsymbol{I}(\tau;\mu,\varphi)}{\mathrm{d}\tau}=-\boldsymbol{I}(\tau;\mu,\varphi)+\frac{\tilde{\omega}(\tau)}{4\pi}\int_0^{2\pi}\int_{-1}^{1}\boldsymbol{M}(\tau;\mu,\varphi;\mu',\varphi')\boldsymbol{I}(\tau;\mu',\varphi')\mathrm{d}\mu'\mathrm{d}\varphi'+\frac{\tilde{\omega}(\tau)}{4\pi}\boldsymbol{M}(\tau;\mu,\varphi;\mu_0,\varphi_0)F_{\mathrm{s}}\exp\left(-\frac{\tau}{\mu_0}\right)\begin{pmatrix}1\\0\\0\\0\end{pmatrix},\tag{1}$$

其中, 矢量$\boldsymbol{I}$表示4个斯托克斯参数$[I, Q, U, V]^{\mathrm{T}}$, I, Q, U, V分别为辐射强度、线偏振方向、线偏振强度和圆偏振分量; $\tilde{\omega}$为单次散射反照率; τ为光学厚度; μ为天顶角余弦, 向下为正; φ表示方位角; μ_0和φ_0分别为太阳入射天顶角余弦以及方位角; F_{s}为大气顶太阳辐射度; $\boldsymbol{M}$为4×4散射矩阵(穆勒矩阵Mueller Matrix), 可由相对于入射光束与散射光束散射平面的相矩阵$\boldsymbol{P}(\cos\Theta)$旋转变换得到. 地气系统辐射圆偏振部分可以忽略, 辐射线偏振度为

$$p=\frac{-Q}{I}.\tag{2}$$

辐射传输方程(1)求解通常采用傅里叶展开的方式, 将辐射强度、散射相矩阵展开为方位角级数求和表示为[14,16]

$$\boldsymbol{I}(\tau;\mu,\varphi)=\sum_{m=0}^{M}\boldsymbol{I}_m^c(\tau;\mu)\cos\left[m(\varphi_0-\varphi')\right]+\boldsymbol{I}_m^s(\tau;\mu)\sin\left[m(\varphi_0-\varphi')\right],\tag{3}$$

$$\boldsymbol{M}(\mu,\varphi;\mu',\varphi')=1/2\boldsymbol{C}_0+\sum_{m=1}^{M}\left\{\boldsymbol{C}_m(\mu,\mu')\cos\left[m(\varphi'-\varphi)\right]+\boldsymbol{S}_m(\mu,\mu')\sin\left[m(\varphi'-\varphi)\right]\right\},\tag{4}$$

式中, $\boldsymbol{M}$为展开级数; $\boldsymbol{C}_m$和$\boldsymbol{S}_m$为傅里叶展开系数; $\boldsymbol{I}_m^s$和$\boldsymbol{I}_m^c$分别表示正、余弦分量. 方程(3)和(4)代入方程(1)得到m阶展开方程为

$$\mu\frac{\mathrm{d}\boldsymbol{I}_m(\tau;\mu)}{\mathrm{d}\tau}=-\boldsymbol{I}_m(\tau;\mu)+\frac{\tilde{\omega}(\tau)}{4}(1+\delta_{0,m})\int_{-1}^{1}\boldsymbol{M}_m(\tau;\mu,\mu')\boldsymbol{I}_m(\tau;\mu,\mu')\mathrm{d}\mu'+\frac{\tilde{\omega}(\tau)}{4\pi}\boldsymbol{M}_m(\tau;\mu,\mu_0)F_{\mathrm{s}}\exp\left(-\frac{\tau}{\mu_0}\right)\begin{pmatrix}1\\0\\0\\0\end{pmatrix},\tag{5}$$

式中, I和Q正弦项为零, U和V余弦项为零, 辐射强度矢量表示为$\boldsymbol{I}_m=\left[I_m^c,Q_m^c,U_m^s,V_m^s\right]^{\mathrm{T}}$(上标$c$表示余弦展开系数, s表示正弦展开系数).

方程(5)求解常用的计算方法有离散坐标法、累加法、逐次散射法等[16~23]. Bai等人[24]基于累加法发展了一套遥感用途的高光谱中短波红外辐射传输精确计算模型, 该模型将地表作为无透射朗伯体层处理, 对大气分层进行近似无限小薄层分层, 通过对薄层反射、透射以及源函数特性累加计算得到地气系统辐射特性. Bai等人[24]的累加法计算模型基于直观物理过程, 计算原理严格, 计算结果稳定, 本文采用该模型开展后续的模拟大气顶卫星观测辐射和分析工作.

1.2 高光谱1.6 μm波段大气顶辐射模拟

近红外1.6 μm波段辐射传输计算需要同时考虑大气气溶胶米散射、分子瑞利散射以及大气分子吸收作用. 假定大气气溶胶在0~60 km高度区间分布, 其消光系数廓线随高度呈指数递减, 根据总光学厚度值整体缩放; 平均消光、散射截面以及散射相矩阵展开系数采用德国不莱梅大学SCIATRAN模型中的

WMO气溶胶模型[25]. 10~60 km高度为背景型气溶胶; 2~10 km高度为大陆型气溶胶; 0~2 km区间为大陆或者城市型气溶胶(本文以下计算假设为城市型气溶胶). 大气分子瑞利散射消光截面根据Bates方法[25]计算得到. 1.6 μm波长气溶胶、分子散射相矩阵展开系数P_{11}以及线偏振系数比$-P_{21}/P_{11}$如图1所示. P_{11}表示散射强度的空间分布特征, 几种气溶胶类型与分子散射前、后向对称特性不同, 表现了明显的前向极大衍射特点; $-P_{21}/P_{11}$表征散射的偏振特征, 在150°~170°区间出现一个负值极值.

大气吸收不会改变辐射的偏振特征, 但吸收强弱的差异会影响辐射在大气中的传播路径, 间接造成不同波长处偏振特性的差异. 本文采用1976年美国标准大气, 考虑大气H_2O, CO_2, O_2等气体吸收, 以及地面朗伯反射假设不引入偏振效应, 利用逐线积分(line-by-line, LBL)方法[26]计算典型大气分子吸收光学厚度, 进而利用累加法[24]计算得到大气顶辐射强度、分子散射产生的线偏振度、气溶胶散射产生的线偏振度. 图2(a)中实线为大气分子吸收总光学厚度, 点实线为大气分子散射总光学厚度, 虚线为气溶胶总光学厚度(550 nm波长处光学厚度为0.3, 下文中如无特殊说明, 光学厚度均为550 nm波长处值). 该波段主要为CO_2吸收作用, 大气分子散射总光学厚度在1.0×10^{-3}量级. 图2(b)为模拟得到的大气顶辐射强度I分量(星下点观测; 太阳高度角为45°; 气溶胶光学厚度0.3; 地表反照率为0.1; 光谱采样点间隔0.004 nm). 图2(c)和(d)分别为忽略气溶胶散射和分子散射计算得到的大气分子散射、气溶胶散射产生的线偏振度. 总体而言, 1.6 μm波段为CO_2弱吸收带, 谱段内大气层顶辐射强度值随吸收的增强而变小, 而散射产生的线偏振则相反, 随着吸收的增强而增强, 此外一般气溶胶散射产生的线偏振度要高于分子散射的线偏振度, 实际计算中需要两者同时的贡献. 需要说明的是, 图2是逐线积分的计算结果, 卷积到卫星光谱仪分辨率后随光谱分辨率的降低该效应会适当减小.

2 忽略偏振辐射误差分析

美国OCO卫星以及我国碳卫星设计, 光谱仪只对主平面辐射垂直分量敏感. 观测辐射量用Stokes参数表示为$1/2(I-Q)$. 忽略偏振计算后, 造成的辐射计算误差可以表示为

$$\mathrm{Error}=\left(\frac{\left(\frac{I_s}{I}\right)}{1-\left(\frac{Q}{I}\right)}-1\right)\times100, \tag{6}$$

式中, I_s为标量辐射传输模拟结果. 误差大小由辐射

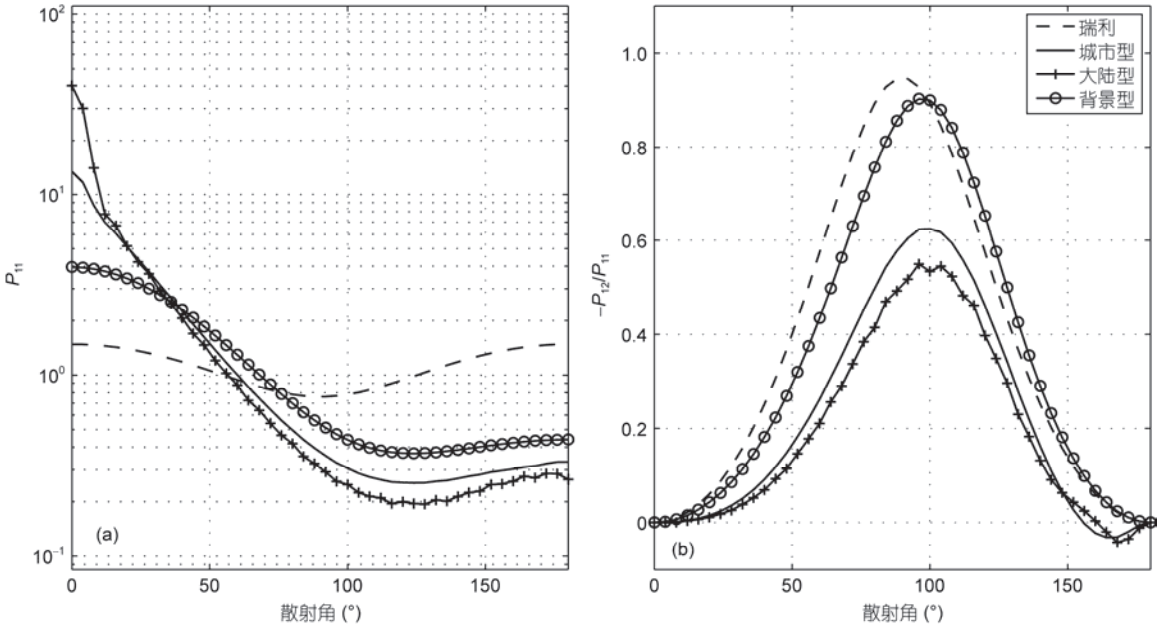


图 1 1.6 μm散射相矩阵中P_{11}项以及线偏振系数比$-P_{21}/P_{11}$

Figure 1 Aerosol scattering phase matrix's item P_{11} and $-P_{21}/P_{11}$ at 1.6 μm

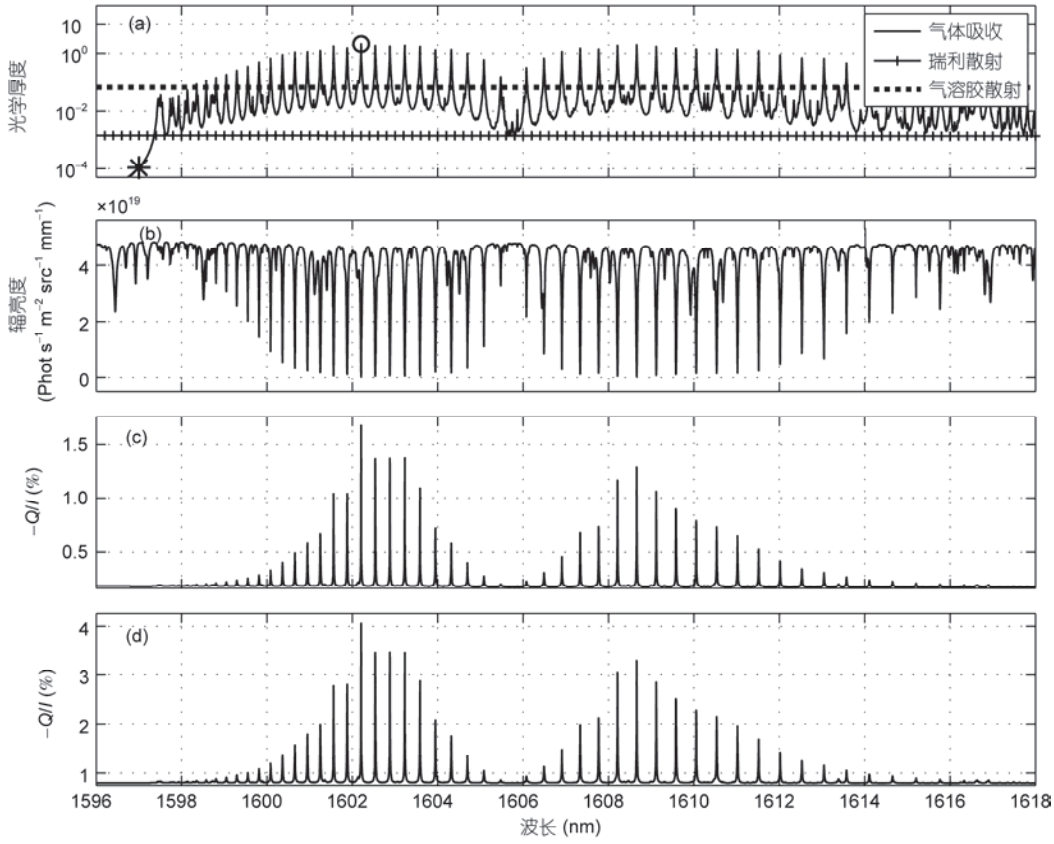


图 2 1.6 μm波段辐射传输计算. (a) 光学厚度; (b) 大气顶辐射强度I分量; (c) 分子散射的线偏振度; (d) 气溶胶散射的线偏振度

Figure 2 Forward model simulation results at 1.6 μm band. (a) Optical depth; (b) intensity I; (c) DOLPs for molecule; (d) DOLPs for aerosol

强度相对偏差和线偏振度大小决定. 一般气溶胶散射条件下, 忽略偏振引入的辐射强度相对偏差I_s/I小于0.5%[12]; Q/I值越大, 误差值越大. 当线偏振度p为正值时, 在100%偏振情况下引起最大误差为50%(忽略I_s/I偏差影响). 在线偏振度为负值情况下, 误差随偏振度值趋向于−100%而变得无限大.

如图3~5为模拟计算得到的在主平面上, 忽略偏振计算导致的辐射模拟误差随观测天顶角的分布, 横坐标为观测天顶角, 负值对应方位角180°, 正值对应方位角0°, 大气廓线保持与2.2节一致. 考虑到气体吸收强弱对辐射偏振度的影响, 选择代表性波长处结果进行比较: 窗区1597.000 nm波长处, 吸收线中心1602.204 nm波长处, 分子吸收光学厚度分别为1.087×10^{-4}和2.126(如图2(a)中星号和圆圈所示).

1.6 μm波段为大气的弱吸收带, 大气顶辐射来自地表反射辐射和大气散射辐射贡献之和. 图3所示在观测角度绝对值小于45°时, 窗区以及吸收线中心波长处辐射强度都随着太阳天顶角减小, 地表直接反射辐射的增强而增大; 偏振度的变化与之相反, 随着太阳天顶角减小, 到达地表辐射增强, 地表朗伯体去极化辐射增强, 相应偏振度减小, 随之忽略偏振计算引入的误差减小. 吸收线位置辐射强度与传输路径以及散射角度有关. 同一太阳天顶角下, 随着观测角度绝对值的增大, 辐射强度明显变小. 而窗区位置辐射与传输路径变化基本无关, 随观测角度的变化相比吸收波段并不明显. 在观测角度绝对值高于45°时, 偏振度随观测角以及太阳天顶角异常变化与来自大气高层的低次散射增强有关[11,12]. 如图4所示, 当观测角度小于50°时, 随着气溶胶光学厚度增大, 到达地表后反射辐射的减弱, 直接散射辐射增强. 窗区位置辐射综合表现为随着气溶胶光学厚度增加而变小, 而吸收线波长处辐射变化与之相反. 观测角度约大于50°情况下, 随散射辐射增强, 窗区辐射表现为随着气溶胶光学厚度增加而变大. 大气顶辐射偏振度随气溶胶光学厚度的变化比较复杂, 一方面随着气溶胶光学厚度增大, 气溶胶内多次散射增强, 从

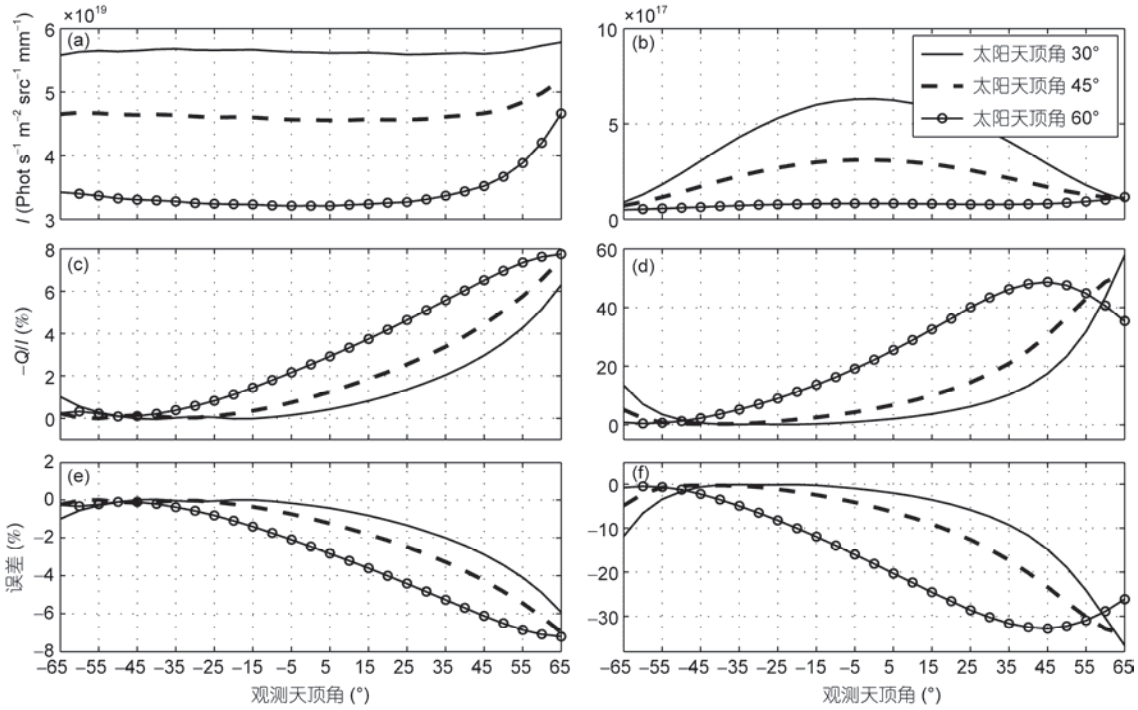


图 3 不同太阳天顶角时, 忽略偏振计算导致的辐射模拟误差随观测天顶角的变化. 气溶胶光学厚度为 0.3; 地表反照率为 0.1. (a), (c), (e) 窗区 1597.0 nm波长处; (b), (d), (f) 吸收线中心 1602.204 nm波长处

Figure 3 Variations of intensity, linear polarization and radiation errors if polarization is neglected at 1597.0 nm (window, (a), (c), (e)) and 1602.204 nm (strong absorption, (b), (d), (f)) as a function of viewing zenith angel. The surface albedo is 0.1. The aerosol optical depth is 0.3

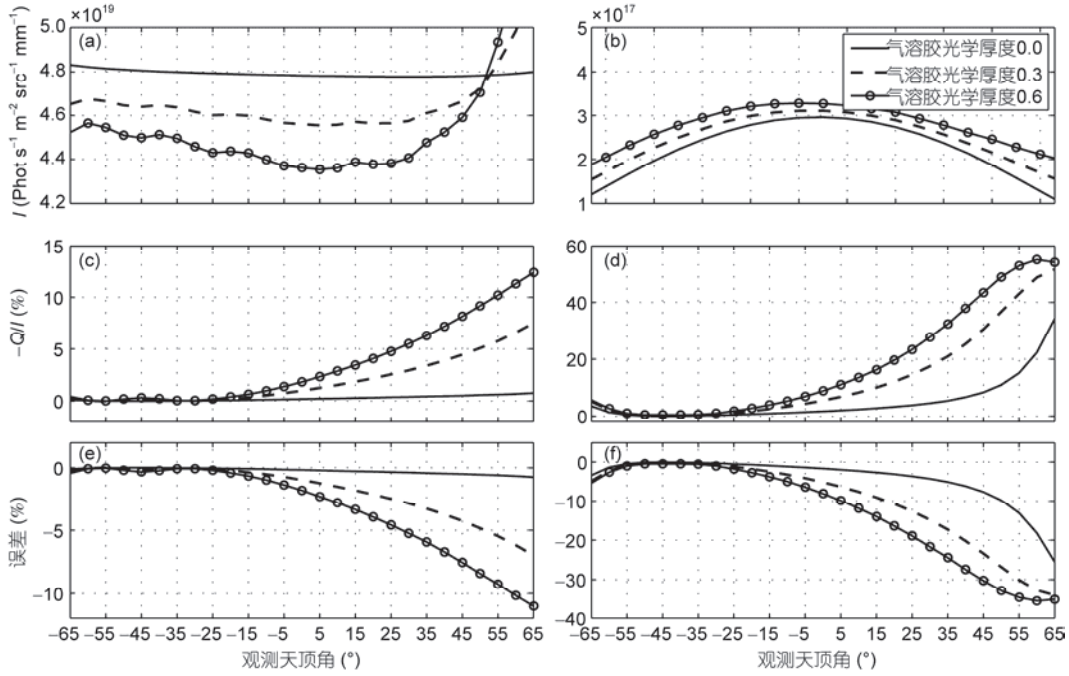


图 4 不同气溶胶光学厚度时, 忽略偏振计算导致的辐射模拟误差随观测天顶角的变化. 太阳天顶角为 45°, 地表反照率为 0.1. (a), (c), (e) 窗区 1597.0 nm波长处; (b), (d), (f) 吸收线中心 1602.204 nm波长处

Figure 4 Variations of intensity, linear polarization and radiation errors if polarization is neglected at 1597.0 nm (window, (a), (c), (e)) and 1602.204 nm (strong absorption, (b), (d), (f)) as a function of viewing zenith angel. The surface albedo is 0.1. The solar zenith angle is 45°

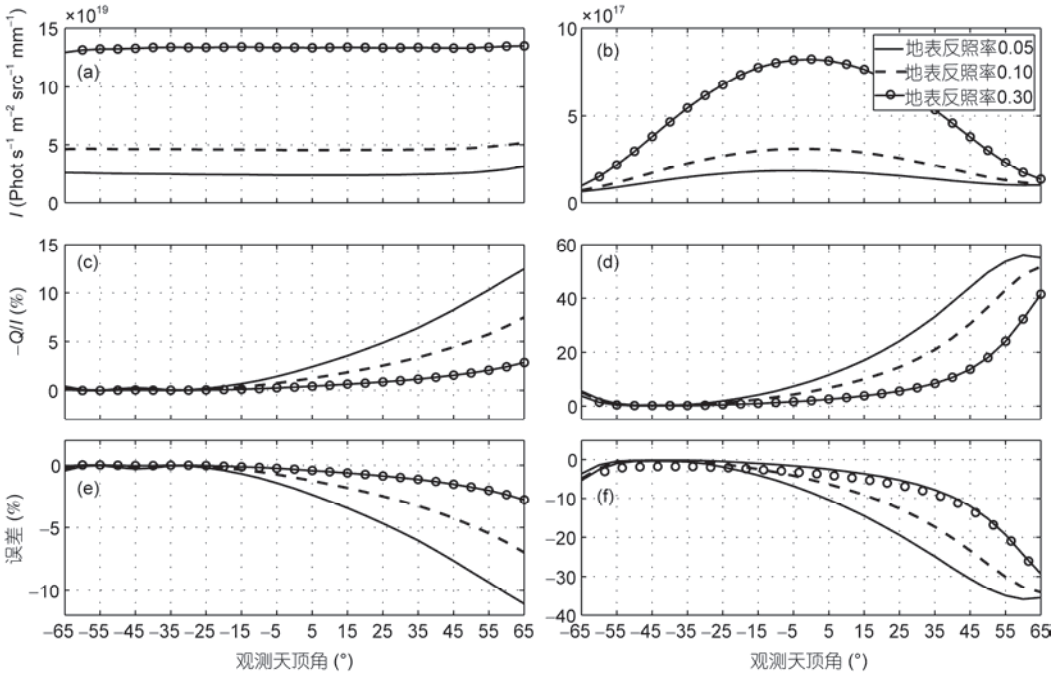


图 5 不同地表反照率时, 忽略偏振计算导致的辐射模拟误差随观测天顶角的变化. 太阳天顶角为 45°, 气溶胶光学厚度为 0.3. (a), (c), (e) 窗区 1597.0 nm波长处; (b), (d), (f) 吸收线中心 1602.204 nm波长处

Figure 5 Variations of intensity, linear polarization and radiation errors if polarization is neglected at 1597.0 nm (window, (a), (c), (e)) and 1602.204 nm (strong absorption, (b), (d), (f)) as a function of viewing zenith angel. The aerosol optical depth is 0.3. The solar zenith angle is 45°

而减弱辐射极化程度; 同时到达地表辐射减弱, 地表的去极化作用会减弱, 大气顶辐射偏振度表现为两者贡献的综合效果. 图4中模拟结果可见, 窗区和吸收线中心偏振度主要受地表去极化程度影响相对较大, 表现为随气溶胶光学厚度增大而增大, 随之忽略偏振造成的辐射计算误差增大. 如图5所示, 随地表反射率升高, 来自地表反射辐射能量的增加, 窗区与吸收线峰值辐射均增大; 相应地表去极化程度变大, 导致偏振度随地表反射率增大而减小, 随之忽略偏振引入的辐射计算误差减小. 受吸收路径变化的影响不同, 吸收线位置相对窗区辐射随观测角度的变化更为敏感.

3 忽略偏振计算引入CO_2反演误差估算

如上模拟分析, 线偏振度随太阳天顶角升高、气溶胶光学厚度增加、地表反照率减少而增加. 相应忽略偏振计算导致的辐射强度计算误差增大, 并且在吸收线波长处要高于窗区波段. 卫星高光谱近红外1.6 μm波段CO_2反演, 通常采用最优估计的方法[27], 即通过对目标参数的非线性迭代实现辐射传输模拟与真实观测的拟合得到. 光谱中包含的CO_2信息来自吸收线位置I_{on_line}与窗区波长处I_{off_line}辐射能量的比值I_{on_line}/I_{off_line}(I_{on_line}, I_{off_line}已采用高斯函数卷积至0.08 nm光谱分辨率, 相当于OCO-2分辨率). 忽略偏振计算导致的该比值的误差表征了由此引入的CO_2反演的误差. 如图6为模拟的星下点观测模式, 不同场景忽略偏振计算以及1 ppmv XCO_2浓度偏差导致的该比值的相对百分比变化, 大气廓线保持与2.2节一致. 由图6(a)可以发现该场景下忽略偏振引入的I_{on_line}/I_{off_line}比值约为1 ppmv引入偏差的2倍, 即相当于约2 ppmv的XCO_2浓度误差. 图6(b)与(a)的区别是地表反照率由0.1增加到0.2, 由于线偏振度随反照率增大而减小, 忽略偏振计算导致的CO_2误差小于图6(a)场景的情况, 约相当于1 ppmv. 图6(c)与(a)的不同是气溶胶光学厚度由0.3增大到0.6, 由于气溶胶散射的增强导致线偏振的增大, 该场景下忽略偏振引入的XCO_2反演误差为3~4 ppmv. 图6(d)与(a)的区别是太阳天顶角增加为60°, 忽略偏振计算导致的XCO_2误差相当于4~5 ppmv.

依据以上CO_2反演偏差估算方法, 对不同太阳天顶角、地表反照率以及气溶胶光学厚度场景下忽略偏振计算的可能引入的XCO_2偏差进行模拟, 结果如图7

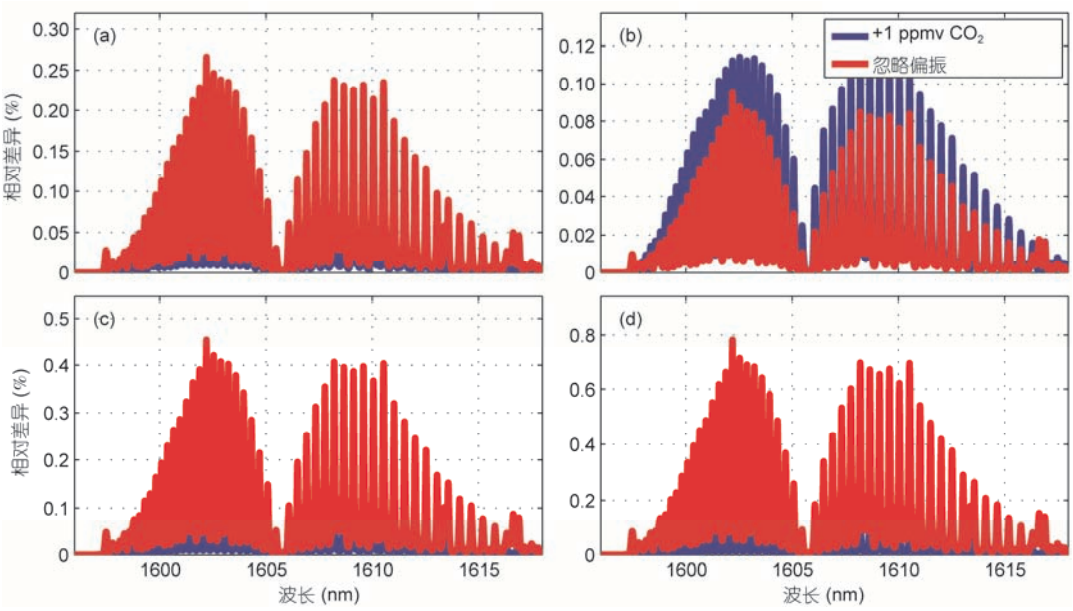


图 6 星下点观测模式, 不同场景忽略偏振计算以及 1 ppmv CO_2 浓度偏差导致的I_{on_line}/I_{off_line}的相对百分比变化. (a) 太阳天顶角 45°, 气溶胶光学厚度 0.3, 地表反照率 0.1; (b) 太阳天顶角 45°, 气溶胶光学厚度 0.3, 地表反照率 0.2; (c) 太阳天顶角 45°, 气溶胶光学厚度 0.6, 地表反照率 0.1; (d) 太阳天顶角 60°, 气溶胶光学厚度 0.3, 地表反照率 0.1. 红线为忽略偏振后导致的比值偏差, 蓝线为整层廓线平移 1 ppmv后引入的比值偏差

Figure 6 The change of the ratio I_{on_line}/I_{off_line} caused by neglecting polarization and 1 ppmv CO_2 profile shifting. (a) The solar zenith angle is 45°, the aerosol optical depth is 0.3 and the surface albedo is 0.1; (b) the solar zenith angle is 45°, the aerosol optical depth is 0.3 and the surface albedo is 0.2; (c) the solar zenith angle is 45°, the aerosol optical depth is 0.6 and the surface albedo is 0.1; (d) the solar zenith angle is 60°, the aerosol optical depth is 0.3, and the surface albedo is 0.1. Red and blue lines represent ratio errors cause by neglecting polarization and 1 ppmv profile shifting

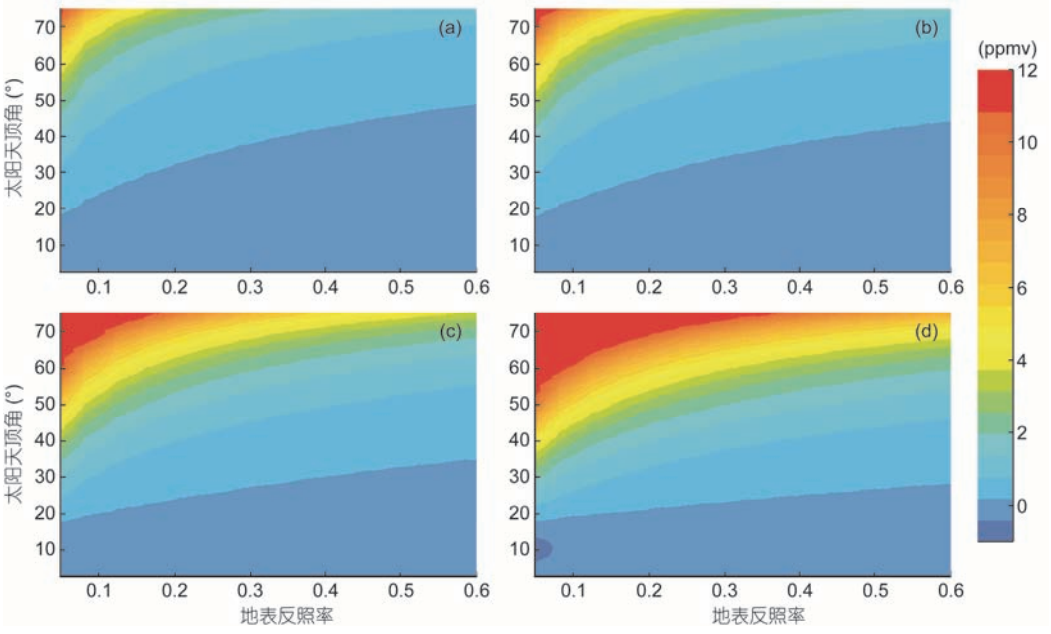


图 7 不同太阳天顶角、地表反照率以及气溶胶光学厚度场景下忽略偏振计算可能引入的XCO_2偏差估算. (a)~(d)分别对应 550 nm波长处气溶胶总光学厚度 0.05, 0.1, 0.3, 0.6. 颜色变化表示CO_2偏差估算值, 大气廓线保持与 2.2 节一致

Figure 7 CO_2 column retrieval errors from ignoring the polarization in forward modeling by linear estimation for different solar zenith angles, surface albedos and aerosol optical depths. (a)–(d) represent aerosol optical depths 0.05, 0.1, 0.3 and 0.6 at 550 nm, respectively. The colors represent CO_2 column retrieval errors. The atmospheric profile is same to Section 2.2

所示，假设为星下点观测，图中可见忽略偏振引入的CO_2反演偏差随太阳天顶角增大、气溶胶光学厚度增加以及地表反射强度减弱而增加：同一气溶胶光学厚度值、同一地表反射率条件下，CO_2反演偏差随太阳天顶角增大而增大．同一气溶胶光学厚度，太阳天顶角条件下，CO_2反演偏差随地表反照率增大而减小；同一太阳天顶角、地表反照率条件下，忽略偏振引入的CO_2反演偏差随气溶胶光学厚度增加而增大．如气溶胶光学厚度为0.05条件下(图7(a))，太阳天顶角小于45°的大部分场景忽略偏振计算导致的XCO_2反演误差小于1 ppmv；而在气溶胶光学厚度0.6(图7(d))，太阳天顶角高于45°，地表反照率小于0.2条件的大部分场景忽略偏振计算可以导致高约5~10 ppmv误差．

图8和9分别为相对方位角180°和0°情况，不同观测角度、地表反照率以及气溶胶光学厚度场景下忽略偏振计算的可能引入的CO_2偏差模拟结果，太阳天顶角设置为45°．除纵坐标表示观测角度外，其他表示与图7相同，大气廓线保持与以上场景一致．图中可见，忽略偏振计算导致的CO_2反演误差分布与图4和5中，线偏振度的变化以及辐射模拟误差相对应．首先在相对方位角180°条件下(图8)：观测天顶角约小于60°时，随观测天顶角增大，地表反照率变大，气溶胶光学厚度的变小，忽略偏振计算导致的CO_2反演误差逐渐减小．例如在气溶胶光学厚度小于0.1，观测角度在30°~60°区间，忽略偏振计算导致的CO_2误差基本小于0.3 ppmv；在气溶胶光学厚度大于0.6，地表反照率小于0.1，观测角度小于5°情况下，忽略偏振计算导致的CO_2误差要高于3~4 ppmv；在观测天顶角高于约60°情况下，同一气溶胶光学厚度条件下，随地表反照率减小，观测角度增大，忽略偏振计算导致的CO_2反演误差逐渐增大．在相对方位角0°条件下(图9)，随观测天顶角增大，地表反照率变小，气溶胶光学厚度的增加，忽略偏振计算导致的CO_2反演误差逐渐增大．

4 结论

本文利用逐线积分方法计算典型大气分子吸收光学厚度，并利用Bai等人[24]发展的累加法模型模拟计算星载仪器近红外1.6 μm波段大气层顶的偏振辐射特征，分析了忽略分子散射和气溶胶散射产生的偏振效应导致的辐射模拟误差以及对大气CO_2反演结果的影响．

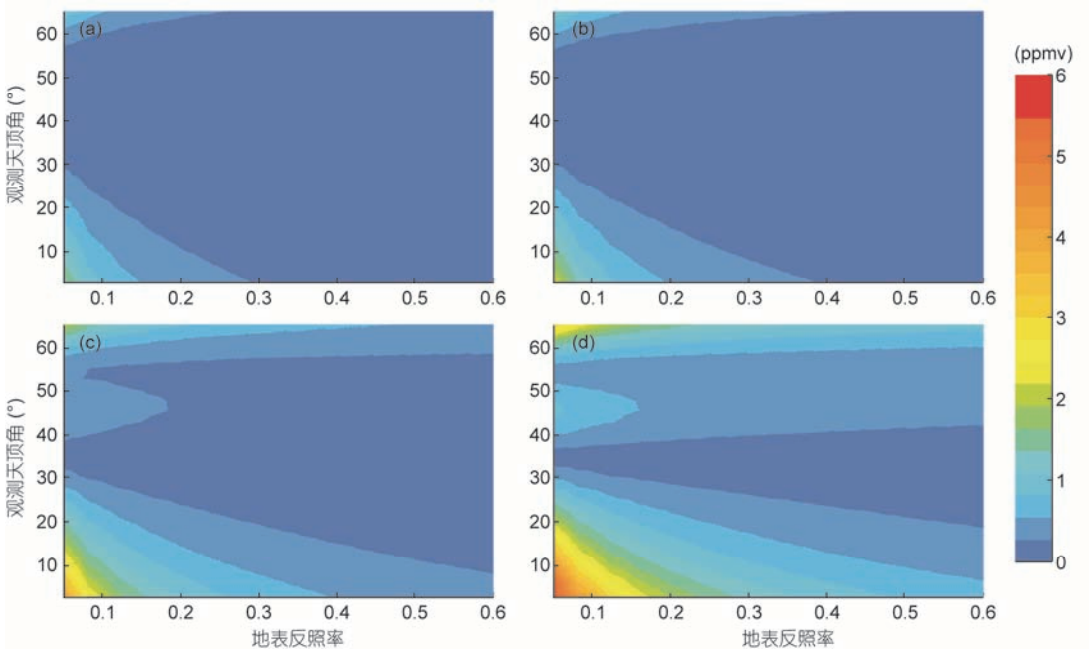


图 8 不同观测天顶角、地表反照率以及气溶胶光学厚度场景下忽略偏振计算的可能引入的CO_2偏差模拟结果．相对方位角 180°，太阳天顶角为 45°，(a)~(d)分别对应 550 nm波长处气溶胶总光学厚度 0.05, 0.1, 0.3, 0.6．颜色变化表示CO_2偏差估算值，大气廓线保持与 2.2 节一致

Figure 8 CO_2 column retrieval errors from ignoring the polarization in forward modeling by linear estimation for different view zenith angles, surface albedos and aerosol optical depths. The relative azimuth angle and the solar zenith angle are 180° and 45°. (a)–(d) represent aerosol optical depths 0.05, 0.1, 0.3 and 0.6 at 550 nm, respectively. The colors represent CO_2 column retrieval errors. The atmospheric profile is same to section 2.2

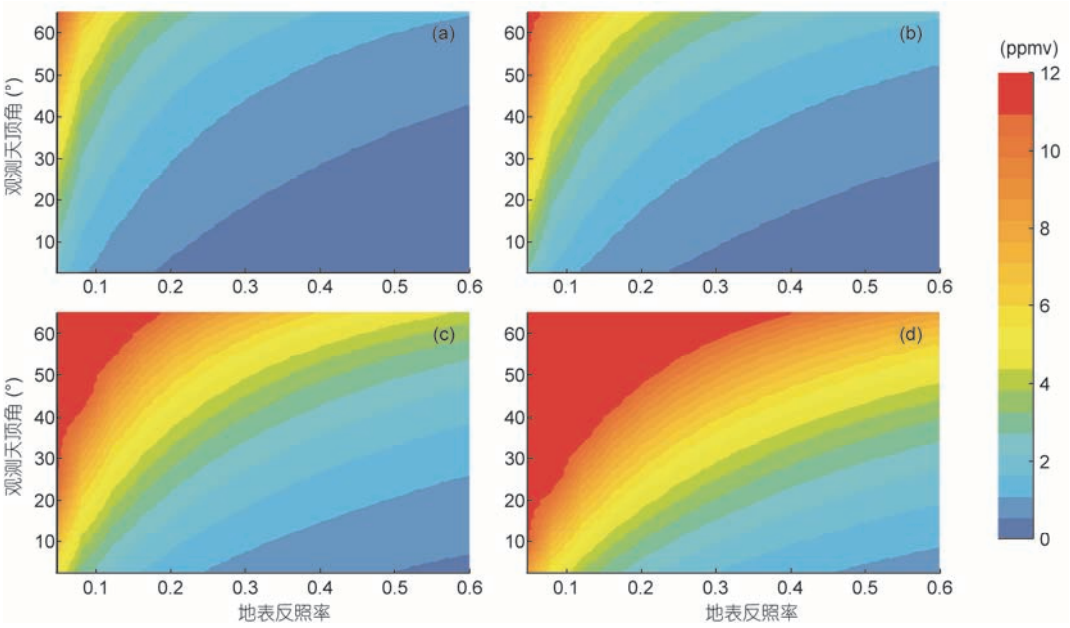


图 9 不同观测天顶角、地表反照率以及气溶胶光学厚度场景下忽略偏振计算的可能引入的CO_2偏差模拟结果. 相对方位角 0°, 太阳天顶角为 45°, (a)~(d)分别对应 550 nm波长处气溶胶总光学厚度 0.05, 0.1, 0.3, 0.6. 颜色变化表示CO_2偏差估算值, 大气廓线保持与 2.2 节一致

Figure 9 CO_2 column retrieval errors from ignoring the polarization in forward modeling by linear estimation for different view zenith angles, surface albedos and aerosol optical depths. The relative azimuth angle and the solar zenith angle are 0.0° and 45°. (a)–(d) represent aerosol optical depths 0.05, 0.1, 0.3 and 0.6 at 550 nm, respectively. The colors represent CO_2 column retrieval errors. The atmospheric profile is same to section 2.2

1.6 μm波段为CO_2气体的弱吸收带, 大气顶辐射来自地表反射辐射和大气散射辐射贡献之和. 本文的研究表明, 同一观测角度下线偏振度随太阳天顶角升高、气溶胶光学厚度增加、地表反照率减少而增加, 忽略偏振计算导致的辐射强度模拟误差增大, 并且吸收线波长处引入的误差量值要高于窗区波长位置.

卫星遥感大气中CO_2浓度信息来自吸收线位置与窗区波长处辐射能量的比值, 本文模拟了不同场景下吸收与窗区通道的辐射能量比值变化, 并对忽略偏振计算造成CO_2反演误差进行了估算, 分析结果表明: 星下点观测模式下, 忽略偏振效应导致的CO_2反演偏差随太阳天顶角增大、气溶胶光学厚度增加以及地表反射强度减弱而增加; 相对方位角180°条件, 同一太阳天顶角下, 除大角度观测天顶角外(太阳天顶角45°时, 值约为60°), 忽略偏振辐射计算导致的CO_2反演偏差随气溶胶光学厚度增加、地表反照强度减弱以及观测角度的减小而升高; 相对方位角0°条件, 同一太阳天顶角下, 忽略偏振辐射计算导致的该CO_2反演偏差随气溶胶光学厚度增加、地表反照强度减弱以及观测角度的增大而升高. 在太阳天顶角大于45°, 气溶胶光学厚度高于0.3, 地表反照率小于0.2的条件下, 多数场景忽略偏振效应导致的XCO_2反演偏差远高于CO_2 1~2 ppmv观测精度需求.

根据本文分析结果, 实现1~2 ppmv反演精度需求, 不仅需要高精度的星载遥感仪器观测, 还需要基于偏振辐射传输计算的高精度观测信号处理.

参考文献

1 Grisp D, Atlas R M, Breon F M, et al. The orbiting carbon observatory (OCO) mission. Adv Space Res, 2004, 34: 700–709

2 Lu N M. Chinese TanSat questions and answers (in Chinese). Democracy Sci, 2017, 1: 44–46 [卢乃锰. 碳卫星问答. 民主与科学, 2017, 1: 44–46]

3 Jiang Y, Yung Y L, Sander S P, et al. Modeling of atmospheric radiative transfer with polarization and its application to the remote sensing of tropospheric ozone. J Quant Spectrosc Radiat Transfer, 2004, 84: 169–179

4 Hasekamp O P, Landgraf J, Van Oss R. The need of polarization modeling for ozone profile retrieval from backscattered sunlight. J Geophys Res, 2002, 107: 4692

5 Mishchenko M I, Travis L D. Satellite retrieval of aerosol properties over the ocean using polarization as well as intensity of reflect sunlight. J Geophys Res, 1997, 102: 16989–17014

6 Duan M Z, Lü D R. Simultaneously retrieving aerosol optical depth and surface albedo over land from POLDER's multi-angle polarized measurement, II: A case study (in Chinese). J Atmos Sci, 2008, 32: 27–35 [段民征, 吕达仁. 利用多角度 POLDER 偏振资料实现陆地上空大气气溶胶光学厚度和地表反照率的同时反演 II: 实例分析. 大气科学, 2008, 32: 27–35]

7 Takano Y, Liou K N. Radiative transfer in cirrus clouds. Part III: Light scattering by irregular ice crystals. J Atmos Sci, 1995, 52: 818–837

8 Levy R C, Remer L A, Kanfman Y J. Effects of neglecting polarization on the MODIS aerosol retrieval over land. IEEE Trans Geosci Remote Sens, 2004, 42: 2576–2583

9 Kuang Z, Margolis J S, Toon G C, et al. Spaceborne measurements of atmospheric CO_2 by high-resolution NIR spectrometry of reflected sunlight: An introductory study. Geophys Res Lett, 2002, 19: 11-1–11-4

10 Boesche E, Stammes P, Bennartz R. Aerosol influence on polarization and intensity in near-infrared O_2 and CO_2 absorption bands observed from space. J Quant Spectrosc Radiat Transfer, 2009, 110: 223–239

11 Stam D M, De Haan J F, Hovenier J W, et al. Degree of linear polarization of light emerging from cloudless atmosphere in the oxgen A band. J Geophys Res, 1999, 104: 16843–16858

12 Natraj V, Spurr R J D, Hartmut B, et al. Evaluation of errors from neglecting polarization in the forward modeling of O_2 band measurements from space, with relevance to CO_2 column retrieval from polarization-sensitive instruments. J Quant Spectrosc Radiat Transfer, 2007, 103: 245–259

13 Liou K N. An Introduction to Atmospheric Radiation II. San Diego: Academic Press, 2002. 317–325

14 Spurr R J D. VLIDORT: A linearized pseudo-spherical vector discrete ordinate radiative transfer code for forward model and retrieval studies in multilayer multiple scattering media. J Quant Spectrosc Radiat Transfer, 2006, 102: 316–342

15 Shi G Y. Atmospheric Radiation (in Chinese). Beijing: Science Press, 2007. 150–157 [石广玉. 大气辐射学. 北京: 科学出版社, 2007. 150–157]

16 Weng F Z, Liu Q H. Satellite data assimilation in numerical weather prediction models. Part I: Forward radiative transfer and Jacobian modeling in cloudy atmospheres. J Atmos Sci, 2003, 60: 2633–2646

17 Siewert C E. A discrete-ordinates solution for radiative-tranfer models that include polarization effects. J Quant Spectrosc Radiat Transfer, 2000, 64: 227–254

18 Zhang P. The theoretic study on the retrieval of aerosol's physical and optical properties from solar spectral reflectance (in Chinese). Doctor Dissertation. Beijing: Institute of Atmospheric Physics Chinese Academy of Sciences, 1998. 53–71 [张鹏. 卫星测量反射太阳光反演气溶胶物理和光学特性的算法研究. 博士学位论文. 北京: 中国科学院大气物理所, 1998. 53–71]

19 Min Q L, Duan M Z. A successive order of scattering model for solving vector radiative transfer in the atmosphere. J Quant Spectrosc Radiat Transfer, 2004, 87: 243–259

20 Lenoble J, Herman M, Deuzé J L, et al. A successive order of scattering code for solving the vector equation of transfer in the Earth's atmosphere with aerosols. J Quant Spectrosc Radiat Transfer, 2007, 107: 479–507

21 Evans K F, Stephens G L. A new polarized atmospheric radiative transfer model. J Quant Spectrosc Radiat Transfer, 1991, 45: 413–423

22 Duan M Z, Min Q L, Lu D R. A polarized radiative transfer model based on successive order of scattering. Adv Atmos Sci, 2010, 27: 891–900

23 Gao Y, Duan M Z, Huang X Y. Preliminary comparisons of the typical polarized radiative transfer models: Precision and efficiency. J Remote Sens, 2010, 14: 845–857

24 Bai W G, Zhang P, Zhang W J, et al. A model for accurately calculating hyper-spectral, middle-shortwave infrared radiative transfer for remote sensing. Sci China Earth Sci, 2018, 61: 317–326

25 Rozanov V V, Rozanov A V, Kokhanovsky A A, et al. Radiative transfer through terrestrial atmosphere and ocean: Software package SCIATRAN. J Quant Spectrosc Radiat Transfer, 2014, 133: 13–71

26 Shephard M W, Clough S A, Payne V H, et al. Performance of the line-by-line radiative transfer model (LBLRTM) for temperature and species retrievals: IASI case studies from JAIVEx. J Atmos Chem Phys, 2009, 9: 7397–7417

27 Rodgers C D. Inverse Methods for Atmospheric Sounding: Theory and Practice. Singapore: World Scientific Publishing, 2000. 66–79

Summary for "忽略 1.6 μm 偏振计算对二氧化碳反演精度的影响"

CO_2 column-retrieval errors arising from neglecting polarization in forward modeling of 1.6 μm band measurements

Wenguang Bai[1,2], Peng Zhang[2*], Wenjian Zhang[2], Gang Ma[2], Chengli Qi[2] & Hui Liu[2]

[1] *School of Atmosphere Physics, Nanjing University of Information Science & Technology, Nanjing 210044, China;*
[2] *National Satellite Meteorology Center, Beijing 100081, China*
* Corresponding author, E-mail: zhangp@cma.gov.cn

Carbon dioxide (CO_2) is a major anthropogenic greenhouse gas. Atmospheric CO_2 has increased from a preindustrial value of about 280 ppmv to more than 400 ppmv, mainly due to the fossil-fuel combustion and changes in land use. Understanding the CO_2 distribution and variability of sources and sinks is essential for predicting changes in future CO_2 concentration. However, *in-situ* measurements collected at a network of surface stations are sparse to allow the CO_2 sources and sinks to be inferred. Satellite remote sensing is one of the best ways to obtain such global observations. The radiances reflected or transmitted by the atmosphere contain information about the atmospheric gases through their absorption signatures. High spectral radiance in the near-infrared 1.6 μm band, observed by OCO and Chinese TanSat, can be used to derive the CO_2 column densities in the atmosphere. Surface reflection and atmospheric scattering processes act to reduce the intensity of radiation polarized in the direction parallel to the principal plane, as defined by the incoming solar beam and the beam entering the instrument. Both the OCO and TanSat instruments are typical polarizing instruments that are designed to measure only the radiation perpendicular to the principal plane; this will create a disparity between the simulation and measurements if polarization effects are neglected in forward modeling.

In this paper, the US standard atmospheric profile with multiple layer aerosol loading is used to evaluate the forward-modeling error made by scalar approximations in the near-infrared 1.6 μm band. Numerical computations were performed using the line-by-line and doubling-adding methods. The atmosphere is assumed to be plane parallel and the surface is set to offer Lambert reflection. The polarizations introduced by molecular Rayleigh scattering and aerosol Mie scattering are calculated respectively. Solar zenith angle, view zenith angle, surface-reflectance, and aerosol optical depth are varied one at a time to evaluate the individual errors. The results show that, except for some situations with very large observation angles, the radiation error made by the scalar approximation increases with the solar zenith angle, increase in aerosol optical depth, and decrease in the surface reflectance. The errors in the line cores are larger than those in the window area because they are affected less by the surface depolarization effect in the absorption channels.

For both OCO and TanSat, the conventional nonlinear least-squares-fitting technique, by which the forward model calculation is fit to satellite observations, is used to obtain the CO_2 column information. The atmospheric CO_2 information comes mainly from the radiation ratio between the absorption and window channels, which means that the radiance-simulation error will be translated into errors in CO_2 column retrieval. To assess these retrieval errors while ignoring the polarization effect in forward mode calculation, sensitivity studies are performed on simulated spectroscopic measurements in the 1.6 μm band. The CO_2-retrieval errors arising from neglecting the polarization effect are seen to be largest when the solar zenith angle is high, the aerosol optical depth is large, and the surface reflectance is low. When the solar zenith angle is larger than 45°, the aerosol optical depth is higher than 0.3 and the surface albedo is less than 0.2; this carbon-dioxide retrieval error could be larger than 1–2 ppmv. Sometimes, this error may be as high as 10 ppmv, making it very large than what is required. The retrieval error budget could thus potentially be dominated by polarization. Thus, to reduce such errors, the forward model needs to take account of fully polarized radiation calculations. On the other hand, it is impractical to do full vector retrieval due to the computational cost. We need to devise ways to quickly complete the polarization radiative-transfer calculation.

vector radiative transfer calculation, satellite measurements in the near infrared 1.6 μm band, carbon dioxide retrieval error

doi: 10.1360/N972017-00853